(Received 9 April 2025, Accepted 26 May 2025, Scheduled 7 June 2025)

Wideband Elliptical Patch Antenna Integrating a Circular Notch and Defected Ground Structure

Bharat D. Prajapati[1, 3, *], Bhavesh Jaiswal[2], and Pravin J. Dalvadi[3]

[1] *Monark University, Gujarat, India*
[2] *Electronics & Communication Engineering Department, Hasmukh Goswami College of Engineering, Gujarat, India*
[3] *Electronics & Communication Engineering Department, Government Polytechnic College, Gandhinagar, India*

ABSTRACT: A circular-slot embedded elliptical patch antenna with DGS ground is introduced for Wi-Fi, Bluetooth, Sub 6 GHz 5G, IRNSS, Wi-Max, and WLAN wireless network applications. The design consists of an elliptical radiating patch featuring a circular cutout positioned on the uppermost layer of the substrate, while the under layer incorporates a DGS structure with two symmetrical slots. The antenna is implemented on an FR4 substrate having a thickness of 1.6 mm and is excited using a microstrip line feed. The structural layout of the antenna corresponds to dimensions of $0.71\lambda \times 0.81\lambda \times 0.016\lambda$. The developed antenna achieved a bandwidth of 86.74%, encompassing a BW extending from 1.73 to 4.38 GHz maintaining a reflection coefficient (S_{11}) lower than -10 dB, exhibiting 5.1 dB of peak gain. The radiation characteristics and surface current density distribution are examined at specific frequencies of 2.4 GHz, 2.78 GHz, 3.5 GHz, and 3.95 GHz. Additionally, the antenna's evolution and parameter effects were examined to better understand its performance characteristics.

1. INTRODUCTION

Slot-integrated printed antennas are gaining popularity in today's wireless network due to their benefits, including low production cost, miniature dimensions, adequate gain, and seamless compatibility with active elements and microwave (MW) circuits. Introducing parasitic patches and shorting vias significantly improves bandwidth and radiation performance. Utilizing coupled microstrips, the miniaturized antenna maintains excellent impedance characteristics [1–3]. Defected Ground Structure (DGS) technique enhances microstrip antenna performance by modifying transmission characteristics, improving impedance bandwidth, and reducing ground copper usage. Slot loading increases bandwidth and miniaturizes the antenna by extending the current path, optimizing gain and resonance frequency [4–6, 13].

This lightweight, wearable textile antenna effectively supports multiple frequency bands for wireless body-area networks. The compact Wi-Fi antenna utilizes a half-mode patch design to ensure precise coverage of unbalanced frequency bands, optimizing performance [7, 8]. Designed for internet of things (IoT) and medical use, this compact, wideband, low-profile antenna utilizes an elastomeric fabric and artificial magnetic conductor. It supports Industrial, Scientific, and Medical (ISM) and Wi-Fi bands. Meander line technique minimizes size but reduces radiation efficiency as antenna dimensions shrink. Ultra-wideband (UWB) antennas are also accumulating significance in medical imaging applications and IoT [9–11].

Several wide-slot configurations have been investigated, including triangular, rectangular, rhombus, elliptical, U-shaped, hexagonal, and octagonal structures. Additionally, the geometry of the patch affects mutual coupling and impedance alignment [12]. Circular notch along with DGS structure provides better bandwidth (BW) improvement than different notch structures like U- and square-shaped slots. It constructively alters paths of current and eliminates surface wave, enhancing impedance matching. Contrasting rectangular notches, a better distribution of current is provided by circular shape [12, 16, 20, 23]. The circularly slotted elliptical patch antenna with defective ground that we present in this communication is examined both experimentally and numerically for a variety of applications. In the beginning, the circular notch and defective structure are applied to the patch and ground, respectively. Additionally, to enhance the antenna's performance, ground plane includes symmetrically placed slots at the corners. The suggested antenna operates from 1.73 GHz to 4.38 GHz, having a 86.74% bandwidth. This antenna demonstrates omnidirectional radiation characteristics in the H-plane and bidirectional radiation patterns in the E-plane. A parametric analysis is conducted to examine the antenna's performance. Furthermore, simulated current distributions of antenna are also described.

2. ANTENNA DESIGN METHODOLOGY

An elliptical patch antenna shown in Figure 1 is an extended version of the circular monopole, characterized by unequal major and minor axes. Higher-order resonances are supported by microstrip antennas, which resemble cavities filled with dielectric material. A more accurate analysis of the electromagnetic fields in the dielectric substrate, which is located in the space

* Corresponding author: Bharat D. Prajapati (bharatdprajapati@gmail.com).

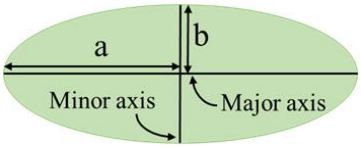

FIGURE 1. Elliptical patch.

separating the patch and the ground, can be achieved by viewing this area as a cavity surrounded by magnetic walls and electric conductors around the edge of the patch. To determine the electromagnetic fields within the cavity, the vector potential method is utilized. For TM^Z modes, the magnetic vector potential A_Z must be first identified, adhering to the homogeneous wave equation in cylindrical coordinates as [12]

$$\nabla^2 A_Z(\rho,\omega,z) + K^2 A_Z(\rho,\omega,z) = 0$$

The dimensions of the elliptical monopole (with the length of major and minor axes — $2a$ and $2b$) are determined and unequal minor and major axes, elliptical patch diverge form circular behavior which in turn leads to the distribution of current nonuniform & mode splitting. This will alter the resonance frequency and initiate multiple resonances, resulting in a wider bandwidth. In contrast to a rectangular patch with sharp edges, elliptical patch with continually shifting curvature provides an intrinsically wider impedance bandwidth, allowing for a smoother surface current distribution and better impedance matching [16, 20, 23]. To calculate the lower operating frequency (f_L) of the electromagnetic (EM) antenna, radius (r) and length (L) of the equivalent cylindrical monopole are calculated by equating its area as follows [12, 23]:

$$2\pi rL = \pi ab$$

The resonant frequencies for TM^Z_{mn0} modes can be expressed as

$$f_r = \frac{1}{2\pi\sqrt{\mu\varepsilon}}\left(\frac{X'mn}{a}\right) \quad (1)$$

The lower frequency f_L can therefore be written as

$$f_L = \frac{C}{L_0\sqrt{\varepsilon_r}} \quad (2)$$

3. THE GEOMETRIC DESIGN OF THE ANTENNA

Figure 2 illustrates the dimensions and geometric design of the suggested antenna. A suggested design is uniform about a longitudinal axis and positioned on the x-y plane. A patch with two elliptical elements, defined by its semi-major axis and semi-minor axis, along with a circular notch (R_{pc}) and microstrip feed line (with length E_{fl} and width E_{fw}), is fabricated on the topmost layer of a substrate. The substrate possesses a thickness of 1.6 mm, dielectric-constant of 4.4, and loss tangent of 0.02. A defective ground structure is incorporated on the substrate's bottom surface, and it is employed to augment antenna performance characteristics, including bandwidth, gain, and mitigating cross-polarization effects. Additionally, two symmetrical parasitic slots (L_{gc} and W_{gc}) are integrated at the vertices of the ground. Antenna's total dimensions

TABLE 1. Geometric parameter values.

Parameter	Value	Parameter	Value
$E1$(Semi major axis)	0.20λ	W_g	0.81λ
$E1$(Semi minor axis)	0.17λ	L_s	0.71λ
$E2$(Semi major axis)	0.24λ	L_g	0.22λ
$E2$(Semi minor axis)	0.12λ	L_{gu}	0.49λ
R_{pc}	0.07λ	W_{gu}	0.02λ
E_{fl}	0.22λ	W_{gc}	0.15λ
E_{fw}	0.03λ	L_{gc}	0.19λ
W_s	0.81λ	R_c	0.02λ

are $0.71\lambda \times 0.81\lambda \times 0.016\lambda$. Table 1 shows the dimensions of the projected design.

In the proposed design, the fundamental mode TM_{00}, where the electrical field is uniformly distributed along the patch, and higher-order modes TM_{10} and TM_{20} are generated in the proposed design which are accountable for the resonance at given frequency.

For fundamental frequency calculations, the elliptical patch antenna is sometimes represented as circular monopole; however, this approximation may result in inconsistencies, particularly when higher frequencies are involved or higher-order modes and impedance matching are taken into account.

4. EVOLUTION OF ANTENNA AND PARAMETRIC ANALYSIS

The evolution of antenna is depicted in Figure 3, and Figure 4 displays an illustration of the frequency responses of antennas 1, 2, 3, and 4. A circular notch is integrated to patch to increase antenna impedance matching, and this notch has two purposes, i.e., tweaking modes and adding the capacitive effect. To optimize antenna performance, the primary antenna is coupled with an additional elliptical radiating patch that is turned at a 90° angle. The ground plane incorporates two symmetrically configured conductive strips that enhance the antenna's operational efficacy. Furthermore, two identical slots are made to maximize the resonating band's return loss and decrease voltage standing wave ratio (VSWR).

Furthermore, a patch antenna's circular notch enhances impedance bandwidth and improves wideband features and performance. Additionally, it improves radiation efficiency and gain by lowering surface wave losses.

It is clearly shown in Figure 4 that a patch antenna incorporating a notch and a defective ground structure (DGS) improves performance by altering the distribution of current and reducing undesired harmonics. The circular notch and slot embedded within the antenna facilitate broadband functionality by meticulously calibrating and optimizing resonance frequency distributions. They collaborate synergistically to enhance radiative efficiency while simultaneously mitigating the surface waves. As shown in Figure 4, the incorporation of a DGS modifies the current flow and disrupts unwanted coupling, leading to improved impedance matching and lowering return loss.

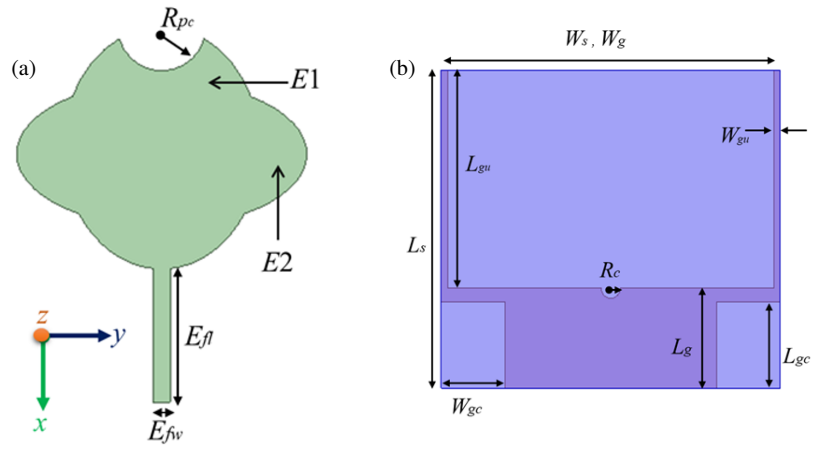

FIGURE 2. Proposed antenna geometry: (a) Top side, (b) bottom side.

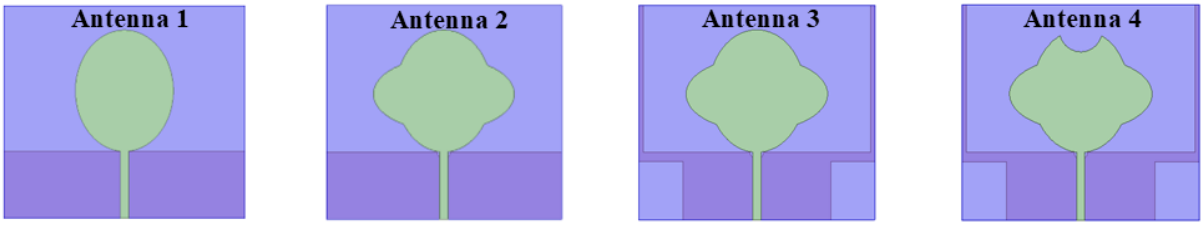

FIGURE 3. Step-by-step antenna evaluation.

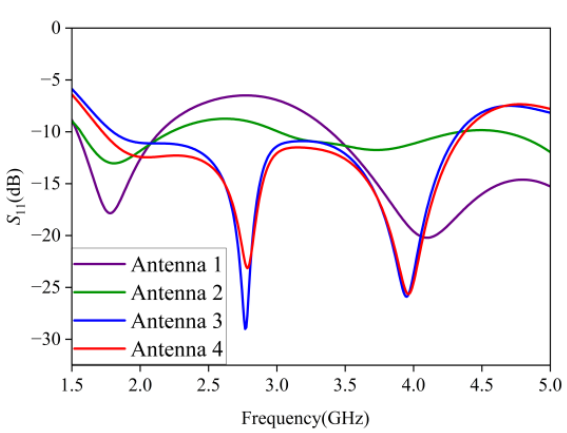

FIGURE 4. Return loss of antenna.

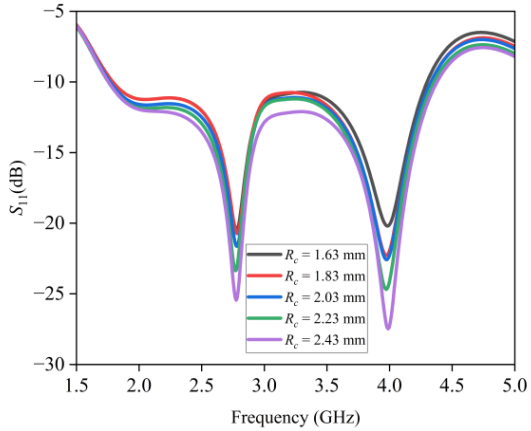

FIGURE 5. Impact of R_c on designed radiating structure.

Figure 5 illustrates the effect of R_c on return loss as R_c varies from 1.63 mm to 2.43 mm. The impedance bandwidth and return loss are improved with an increase in R_c. The augmentation of R_c contributes to the enhancement of impedance bandwidth while efficiently enhancing return loss.

Figure 6 clearly demonstrates that increasing the value of L_{gc} leads to an enhancement in the impedance bandwidth (IBW) of designed antenna while improving return loss. The variation in W_{gc} on frequency response curve (FRC) is depicted in Figure 7. The upper cutoff frequency undergoes modification, concurrently enhancing the return loss within the range of mid-frequency. As shown in Figure 8, both lower and upper cutoff frequencies move to the right as W_{gu} increases from 0.7 mm to 2.3 mm.

The lower cutoff frequency is determined using Equation (2), where Lo represents the distance in Figure 9 and $Lo = L_1 + L_2 + L_3$. Lower cutoff frequencies 1.68 GHz and 1.73 GHz have been calculated and simulated. A minor discrepancy of 2.28% is observed between the calculated and simulated lower cutoff frequencies.

5. RESULTS AND DISCUSSION

Figure 10 demonstrates the suggested antenna prototype. The proposed microstrip patch antenna (MPA) is simulated using High Frequency Structure Simulator (HFSS), while fabricated MPA is evaluated inside an anechoic chamber, as depicted in Figure 11. Investigation evaluates reflection coefficient, pat-

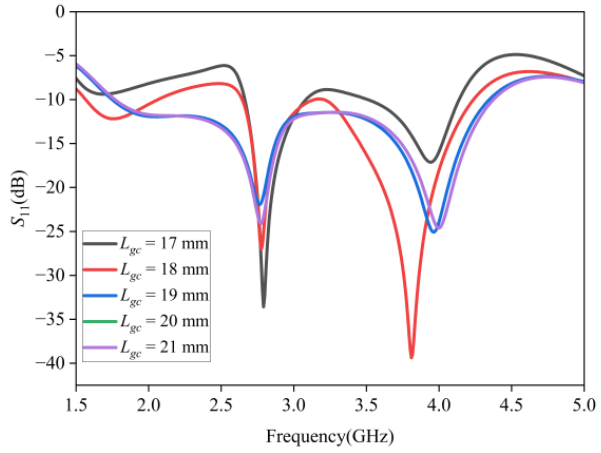

FIGURE 6. Impact of L_{gc} on the designed radiating structure.

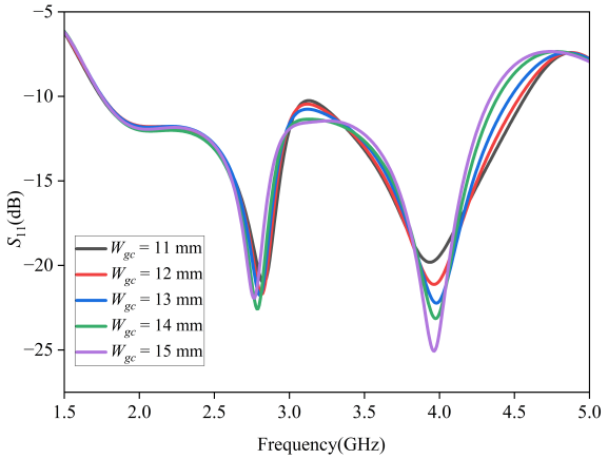

FIGURE 7. Impact of W_{gc} on designed radiating structure.

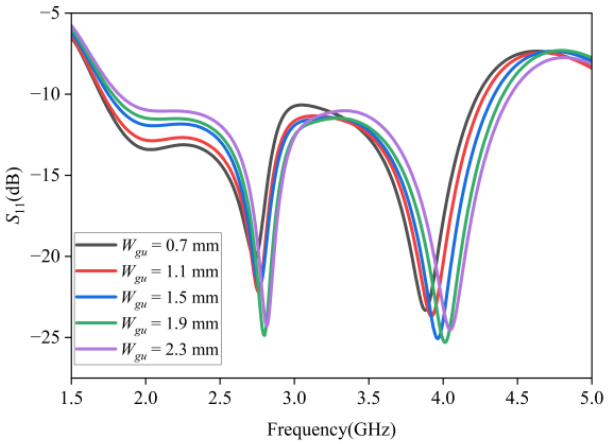

FIGURE 8. Impact of W_{gu} on designed radiating structure.

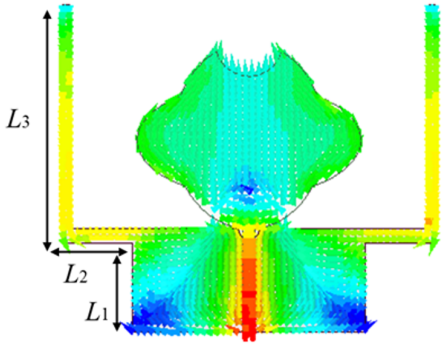

FIGURE 9. Surface current distribution at the lower cutoff frequency.

FIGURE 10. Antenna prototype.

tern of radiation, gain, and VSWR, comparing the measured results with simulation outcomes.

A comparison of simulated and measured S_{11} (Reflection coefficient) and VSWRs against frequency are shown in Figure 12 and Figure 13.

As depicted in the figures, the high degree of agreement and consistency is observed. The developed antenna achieved a bandwidth of 2.65 GHz (86.74%), encompassing a BW extending from 1.73 to 4.38 GHz for maintaining a reflection coefficient (S_{11}) lower than -10 dB. The discrepancy between measured and simulated return losses is caused by manufacturing deviations, SMA connector, and the influence of the ground plane.

Figure 14 illustrates the distribution of surface current along frequencies. The antenna exhibits a well-defined current distribution, ensuring efficient excitation and controlled radiation characteristics. Strong coupling is indicated by a high current density at the feed, which maximizes power transfer and raises antenna efficiency overall.

The normalized current configuration and the far-field radiation distribution in both E-plane (XZ plane, $\Phi = 0°$) and H-plane (YZ-plane, $\Phi = 90°$) are presented in the corresponding Figure 15. It shows the radiation patterns of the proposed antenna at the frequencies of 2.4, 2.78, 3.5, and 3.96 GHz. The radiation pattern exhibits a well-defined bidirectional characteristic in the X-Z plane, enhancing focused signal transmission. In contrast, the near-omnidirectional behavior in the Y-Z plane ensures broader coverage and consistent performance.

Table 2 presents comparative performance analysis of the designed antenna alongside various reported designs, evaluating aspects such as dimensions, bandwidth, gain, radiation efficiency, frequency range, and feeding techniques. Figure 16 presents the measured gains of 3.2 dB, 4 dB, 3.3 dB, and 5.1 dB for the proposed antenna across various frequencies. The simulated radiation efficiency of proposed antenna varies form 88 to 96%.

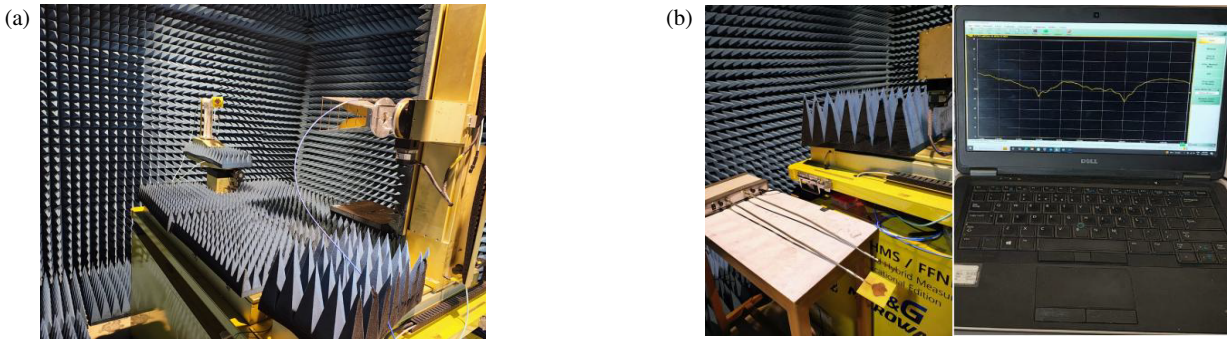

FIGURE 11. (a), (b) Anechoic chamber setup for measuring the proposed antenna.

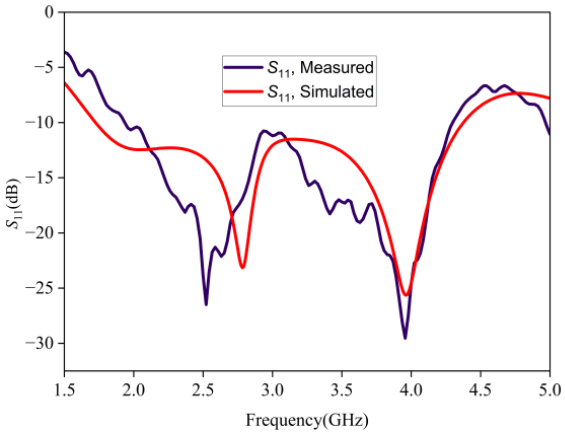

FIGURE 12. Measured and simulated reflection coefficients.

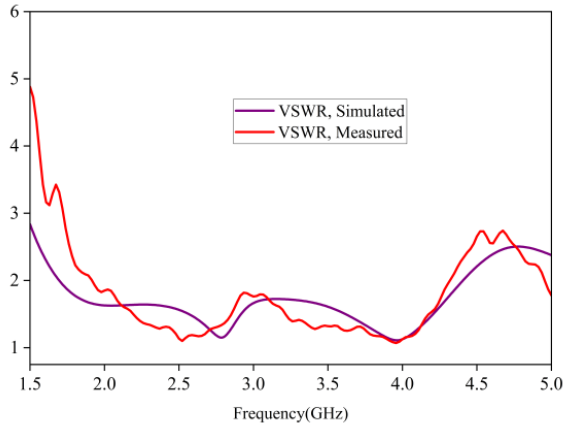

FIGURE 13. Measured and simulated VSWRs.

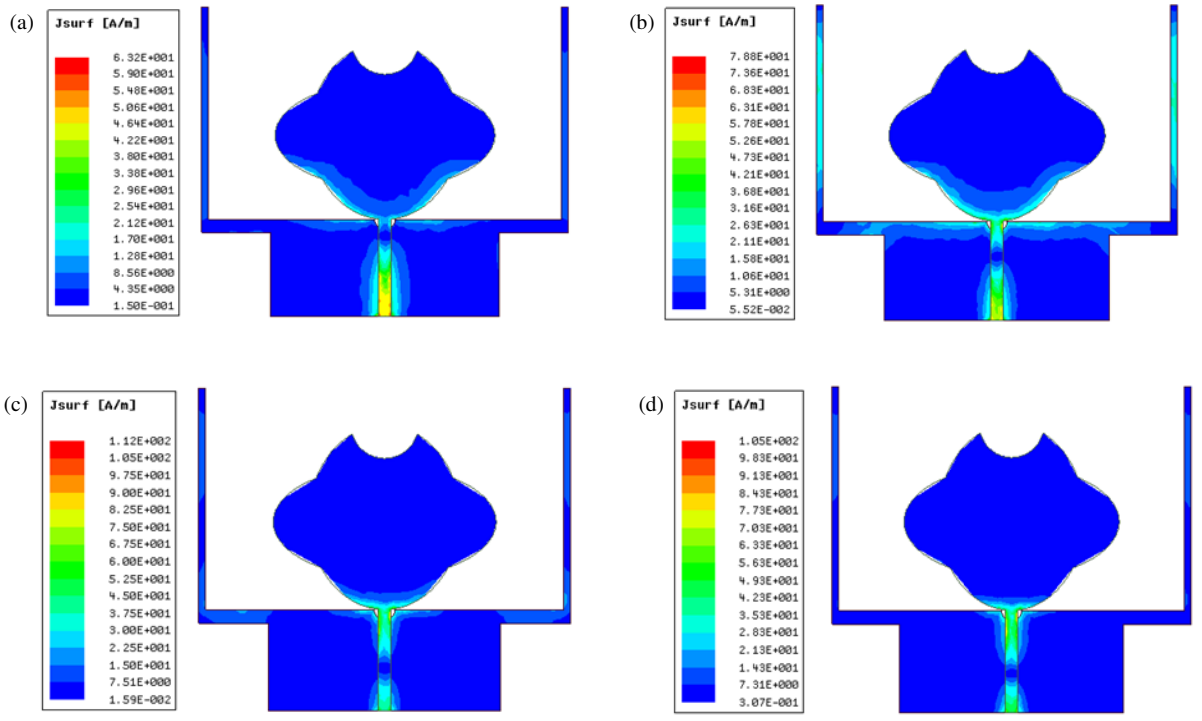

FIGURE 14. Impact of surface current distribution. (a) 2.4 GHz, (b) 2.78 GHz, (c) 3.5 GHz, (d) 3.95 GHz of proposed antenna.

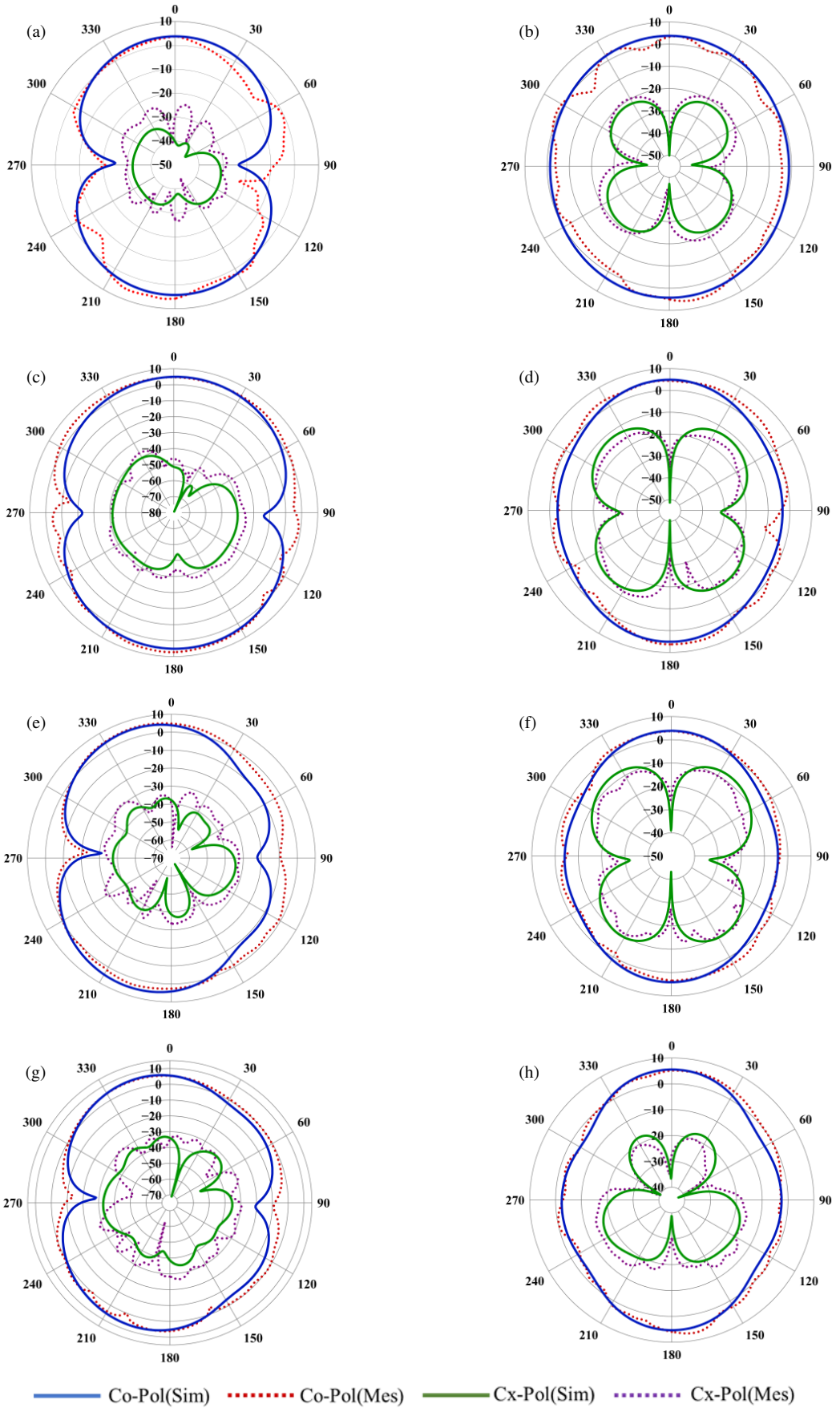

FIGURE 15. Measured and simulated far-field radiation patterns of the designed antenna. (a) 2.4 GHz-E field, (b) 2.4 GHz-H field, (c) 2.78 GHz-E field, (d) 2.78 GHz-H field, (e) 3.5 GHz-E field, (f) 3.5 GHz-H field, (g) 3.95 GHz-E field, (h) 3.95 GHz-H field.

TABLE 2. Comparison of the proposed antenna's performance with that of the reported antenna.

Ref.	Size	Frequency Range (GHz)	BW (%)	Substrate	Technique-Feeding	Efficiency (∼ %)	Gain
[14]	$0.60\lambda \times 0.60\lambda \times 0.003\lambda$	1.42–1.56	9	Roger 4350B	HMSIW/QMSIW	-	7 dBic
[15]	$0.53\lambda \times 0.53\lambda \times 0.013\lambda$	2.1–3.2	41.5	FR4	CPW	-	3 dBi
[16]	$0.14\lambda \times 0.26\lambda \times 0.011\lambda$	1.42–2.52	55.83	FR4	Tapered Microstrip	93.16%	5.55 dBi
[17]	$0.96\lambda \times 1.93\lambda \times 0.01\lambda$	3.2–4.5	33.76	FR4	Microstrip	70–82%	4.25 dB
[18]	$1.1\lambda \times 1.1\lambda \times 0.05\lambda$	3.96–5.73	36.5	Roger	CPW	90–93%	10.45 dBi
[19]	$1.93\lambda \times 1.03\lambda \times 0.01\lambda$	3.4–4.3	23.4	FR4	Coaxial	43%	3 dBi
[20]	$0.65\lambda \times 0.62\lambda \times 0.27\lambda$	4.5–5.75	24.4	FR4	Microstrip	81%	6 dBi
[21]	$0.82\lambda \times 0.82\lambda \times 0.34\lambda$	3.3–5	40.9	FR4	Microstrip	55–82%	4.4 dBi
[22]	$0.42\lambda \times 0.42\lambda \times 0.013\lambda$	1.70–3.34	65.1	FR4	Microstrip	75%	5.49 dBi
This work	$0.71\lambda \times 0.81\lambda \times 0.016\lambda$	1.73–4.38	86.7	FR4	Microstrip	88–96%	5.1 dB

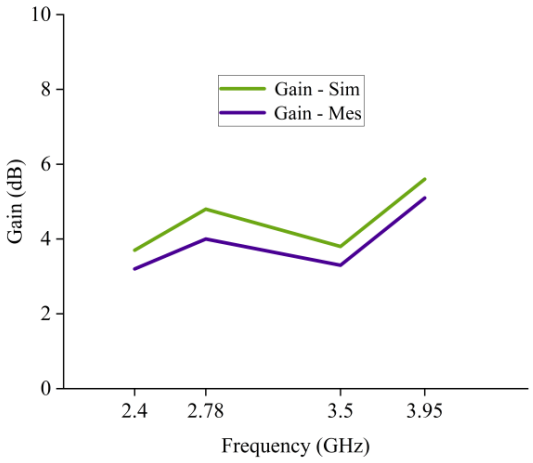

FIGURE 16. Measured and simulated gains of the designed antenna.

6. CONCLUSION

An elliptical patch antenna having a circular notch fed by a microstrip line for wideband application is investigated. The developed antenna achieved a bandwidth of 86.74%, covering a frequency range from 1.73 to 4.38 GHz for maintaining a reflection coefficient (S_{11}) lower than -10 dB, and the distributions of surface currents and associated radiation patterns were analyzed at resonance frequencies of 2.4 GHz, 2.78 GHz, 3.5 GHz, and 3.95 GHz, achieving maximum gains of 3.2 dB, 4 dB, 3.3 dB, and 5.1 dB. At all frequencies, the far-field pattern is bidirectional and omnidirectional, and there is a slight variation between the observed and simulated radiation patterns. The antenna's evolution and the impact of parameters are also examined.

ACKNOWLEDGEMENT

We sincerely thank Entuple Technologies Pvt. Ltd., Ahmedabad, Gujarat, India, for providing access to their anechoic chamber for testing the proposed work.

REFERENCES

[1] Sacco, G., P. D'Atanasio, and S. Pisa, "A wideband and low-sidelobe series-fed patch array at 5.8 GHz for radar applications," *IEEE Antennas and Wireless Propagation Letters*, Vol. 19, No. 1, 9–13, Jan. 2020.

[2] Xu, K. D., H. Xu, Y. Liu, J. Li, and Q. H. Liu, "Microstrip patch antennas with multiple parasitic patches and shorting vias for bandwidth enhancement," *IEEE Access*, Vol. 6, 11 624–11 633, 2018.

[3] Shao, Z. and Y. Zhang, "A single-layer miniaturized patch antenna based on coupled microstrips," *IEEE Antennas and Wireless Propagation Letters*, Vol. 20, No. 5, 823–827, May 2021.

[4] Sharma, S. and M. Kumar, "A millimeter wave elliptical slot circular patch MIMO antenna for future 5G mobile communication networks," *Progress In Electromagnetics Research M*, Vol. 110, 235–247, 2022.

[5] Seng, T. K., T. K. Geok, H. A. Ghani, C. J. Kit, and L. L. Hong, "Microstrip antenna design for ultra-wideband frequency," in *2017 International Conference on Robotics, Automation and Sciences (ICORAS)*, 1–5, Melaka, Malaysia, 2017.

[6] Musa, U., S. M. Shah, H. A. Majid, I. A. Mahadi, M. K. A. Rahim, M. S. Yahya, and Z. Z. Abidin, "Design and analysis of a compact dual-band wearable antenna for WBAN applications," *IEEE Access*, Vol. 11, 30 996–31 009, 2023.

[7] Li, H., J. Du, X.-X. Yang, and S. Gao, "Low-profile all-textile multiband microstrip circular patch antenna for WBAN applications," *IEEE Antennas and Wireless Propagation Letters*, Vol. 21, No. 4, 779–783, Apr. 2022.

[8] Gao, S., L. Chang, A. Zhang, Y. Li, and Z. Zhang, "Small-volume microstrip patch antennas exactly covering Wi-Fi 6 bands of 2.4–2.5 GHz and 5.15–5.85 GHz," *IEEE Transactions on Antennas and Propagation*, Vol. 71, No. 7, 5739–5748, Jul. 2023.

[9] Islam, M. S., M. T. Islam, M. A. Ullah, G. K. Beng, N. Amin, and N. Misran, "A modified meander line microstrip patch antenna with enhanced bandwidth for 2.4 GHz ISM-band Internet of Things (IoT) applications," *IEEE Access*, Vol. 7, 127 850–127 861, 2019.

[10] Chen, X., Y. Wei, Y. Li, Z. Liang, S. Y. Zheng, and Y. Long, "A gain-enhanced patch antenna with a periodic microstrip rampart line," *IEEE Open Journal of Antennas and Propagation*, Vol. 3, 83–88, 2021.

[11] Dey, A. B., S. Kumar, W. Arif, and J. Anguera, "Elastomeric textile substrates to design a compact, low-profile AMC-based antenna for medical and IoT applications," *IEEE Internet of Things Journal*, Vol. 10, No. 6, 4952–4969, Mar. 2023.

[12] Balanis, C. A., *Antenna Theory: Analysis and Design*, John Wiley & Sons, Hoboken, New Jersey, 2016.

[13] Prajapati, B. D. and B. Jaiswal, "Comprehensive analysis of microstrip patch antenna for wireless application," *Indian Journal of Natural Sciences*, Vol. 15, No. 87, Dec. 2024.

[14] Sun, K., Y. Tang, S. Liu, J. Pan, and D. Yang, "A wideband circularly polarized microstrip patch antenna with embedded shielding package based on quarter-mode substrate integrated waveguide feed," *IEEE Access*, Vol. 8, 140 524–140 532, 2020.

[15] Birwal, A., V. Kaushal, and K. Patel, "Investigation of circularly polarized CPW fed antenna as a 2.45 GHz RFID reader," *IEEE Journal of Radio Frequency Identification*, Vol. 6, 593–600, 2022.

[16] Devana, V. N. K. R., S. C. Sekhar, V. L. N. P. Ponnapalli, G. S. Reddy, N. Radha, *et al.*, "A compact MIMO antenna for GPS/PCS/Bluetooth wireless applications," in *2023 3rd International Conference on Intelligent Technologies (CONIT)*, 1–4, Hubli, India, 2023.

[17] Abdullah, M., S. H. Kiani, N. Shoaib, T. Ali, H. Elmannai, A. D. Algarni, and U. F. Khattak, "An eight element wideband DGS MIMO antenna system for 5G handheld devices," *IEEE Access*, Vol. 12, 141 476–141 488, 2024.

[18] Sun, W., Y. Li, Z. Zhang, and P.-Y. Chen, "Low-profile and wideband microstrip antenna using quasi-periodic aperture and slot-to-CPW transition," *IEEE Transactions on Antennas and Propagation*, Vol. 67, No. 1, 632–637, Jan. 2019.

[19] Qian, L., X. Chen, X. Liu, H. Zhou, H. Wang, and M. Hou, "Low-profile wideband patch antenna using even and odd modes for 5G terminal applications," *IEEE Antennas and Wireless Propagation Letters*, Vol. 23, No. 8, 2476–2480, Aug. 2024.

[20] Ghouz, H. H. M., M. F. A. Sree, and M. A. Ibrahim, "Novel wideband microstrip monopole antenna designs for WiFi/LTE/WiMax devices," *IEEE Access*, Vol. 8, 9532–9539, 2020.

[21] Hu, M. and Y. Li, "Wideband back cover microstrip antenna with multiple shorting vias for mobile 5G MIMO applications," *IEEE Transactions on Antennas and Propagation*, Vol. 71, No. 10, 8290–8295, Oct. 2023.

[22] Xue, J., A. Ni, L. Liu, Z. Wang, and X. Wang, "An ultra-wideband antenna based on left-handed materials for IoT applications," *Progress In Electromagnetics Research C*, Vol. 140, 151–161, 2024.

[23] Kumar, G. and K. P. Ray, *Broadband Microstrip Antennas*, Artech House, Norwood, 2003.